Radial diffraction strength and elastic behavior of CaF_2 in low- and high-pressure phases

Abby Kavner*
Earth & Space Sciences Department and Institute for Geophysics and Planetary Physics, University of California, Los Angeles, Los Angeles, California 90095, USA

(Received 18 March 2008; revised manuscript received 25 April 2008; published 4 June 2008)

The radial-diffraction lattice behavior of CaF_2 was analyzed in its low-pressure (fluorite) and high-pressure phase up to 11.5 GPa using radial x-ray diffraction techniques in the diamond anvil cell. Between 3.5 and 7.1 GPa, fluorite develops a radial-diffraction strength of ~0.8 GPa. The corresponding lattice anisotropy of the fluorite phase was measured to be equal to 0.73, in good agreement with previous Brillouin spectroscopy measurements. By 8.8 GPa, CaF_2 has undergone a phase transformation to its high-pressure (orthorhombic) phase, with a corresponding volume decrease of 10.4%. By 11.5 GPa, the volume drop between the low-pressure and high-pressure phase has increased to 11.5%. In addition, the high-pressure phase is found to withstand a significantly larger differential stress than the low-pressure fluorite phase, with a large degree of lattice anisotropy. In the maximum stress direction at 8.8 GPa, we observe a time-dependent evolution of the lattice parameters of CaF_2, indicating that the high-pressure structure is still undergoing deformation on time scales of hours after the phase boundary has been crossed.

DOI: 10.1103/PhysRevB.77.224102 PACS number(s): 62.50.−p, 61.05.cp, 62.20.F−, 64.60.−i

I. INTRODUCTION

Halides have a variety of important roles in high-pressure materials science. First, they serve as test materials for condensed matter theoretical predictions of the behavior of ionic materials. Second, since halides are more compressible than oxides and silicates, phenomena involving large lattice strains can be observed over a relatively narrow pressure range. Therefore, they have long been used as mineralogical models for the behavior of ionically bonded minerals in the Earth's mantle and as test materials for the development of high-pressure equations of state.[1] The halides undergo pressure-induced phase transformations and therefore help constrain theories for phase stability, and experiments exploring these transformations aid in our understanding of phase transformations in the deep Earth. Finally, because they have been well studied and because they are usually elastically compressible, the halides are commonly used as standard materials for the study of high-pressure and high-temperature material behavior.[2,3] Most of our effort in understanding halide behavior involves studying these materials under hydrostatic conditions; however, material behavior under mechanical disequilibrium is relevant to understanding material strength, transport properties, and mechanisms of phase transformations. Therefore, the goal of this work is to use radial-diffraction techniques to examine the high-pressure lattice strain behavior of the halide CaF_2 under extremely nonhydrostatic conditions.

At pressures up to ~9 GPa, CaF_2 is stable in the fluorite structure, which consists of a close-packed cubic Ca lattice, with F^- occupying the tetrahedral sites. As theoretically predicted[4,5] and experimentally determined, CaF_2 fluorite undergoes a phase transformation to an orthorhombic structure (*Pnma*, similar to the $PbCl_2$ "cotunnite" structure) at a pressure between 8 and 10 GPa.[6–8] Both the fluorite and the cotunnite structures are based on close-pack Ca lattice. However, in the fluorite structure, the Ca sublattice is based on a cubic close packing, with the F^- occupying all of the tetrahedral interstices. The high-pressure ($PbCl_2$) structure of fluorite is also based on a close-pack cation structure, but with a distorted hexagonal lattice, and with F^- ions in the tetrahedral (fourfold) and off-octahedral (fivefold) interstices.[7]

For a material subjected to large nonhydrostatic stresses in the diamond anvil cell, radial-diffraction techniques measure lattice-plane strain as a function of direction from minimum to maximum stress, which allows experimental access to several bits of information, including a bound on the materials elastic yield strength, lattice-dependent strain indicating anisotropy, and a measure of a material's pressure-volume equation of state. CaF_2 is especially interesting to investigate using these techniques because its strength and elastic properties can be examined before, during and after a pressure-induced phase transformation. The lattice-dependent behavior of halides as they undergo a phase transformation during nonhydrostatic deformation will extend our understanding of materials at phase transformations in general and specific to the interior of the Earth, which is important since phase transformations help control the dynamic behavior of the mantle.

II. EXPERIMENTAL PROCEDURE

Radial-diffraction experiments were performed at beam line X17C of the National Synchrotron Light Source using experimental procedures similar to ones describe previously.[9–14] Polycrystalline fluorite (CaF_2) and gold powder in a ~10:1 ratio were mixed and loaded in a preindented and drilled beryllium gasket and then pressurized in a symmetric diamond anvil cell. Energy-dispersive x-ray diffraction experiments in the radial geometry were performed with a constant diffraction angle of $2\theta = 10.00(3)°$, calibrated by fluorescent standards and a gold foil at ambient conditions.

At each of the pressure steps, a series of energy-dispersive diffraction patterns were obtained of the center part of the sample. The geometry of the incoming and diffracted x-ray

beam was maintained parallel to and in between the diamond faces through an x-ray transparent beryllium gasket. The diamond cell was rotated about the angle bisector between the direct beam and the diffracted beam ψ. This geometry provides a method to collect x-ray diffraction patterns from subsets of lattice planes as a function of orientation with respect to the stress tensor imposed by the diamond cell geometry. At $\psi=90°$, the measured lattice strains are responding to the maximum principal stress, aligned along the diamond compression axis. At $\psi=0°$, the lattice strains are responding to the minimum principal stress, which is supplied by the gasket. Other rotations of the diamond anvil cell sample intermediate combinations of maximum and minimum stress direction. Since the diamond anvil cell sample chamber is assumed to be cylindrically symmetric about the diamond compression axis, a hydrostatic lattice response is calculated at $\psi=54.7°$.

Diffraction patterns were collected at six pressure steps for a total of 35 diffraction patterns. At the fifth pressure step, a series of diffraction patterns sampling the maximum strain direction were collected at times ranging from 3 min to 12 h to evaluate potential time dependence. Lattice planes of both polycrystalline CaF_2 and Au within the diamond cell respond to stresses imposed by the diamond cell and the surrounding polycrystalline matrix. Typical x-ray diffraction patterns of Au and CaF_2 in the minimum and maximum stress directions are shown in Figs. 1(a) and 1(b).

III. DATA ANALYSIS

To analyze the data, we used a linear elasticity theory that accounts for lattice-dependent strain behavior in a polycrystalline assemblage subject to a cylindrically symmetric, nonhydrostatic stress state in the diamond anvil cell.[14,15] The assumptions are that each set of lattice planes experiences a directional strain depending in its orientation in the diamond cell sample chamber, with respect to a cylindrically symmetric stress state oriented with the maximum and minimum principal stress directions along the diamond normal axis and the gasket direction, respectively. Using Hooke's law and the diamond anvil cell geometry and simplifying assumptions mentioned above, the relationship between the measured d-spacings $d(hkl)$ and the azimuthal angle ψ derived by Singh and co-workers[14,15] is given by

$$d(hkl) = d_{\text{hydro}}[1 + (1 - 3\cos^2\psi)Q(hkl)], \tag{1}$$

where d_{hydro} is the d spacing corresponding to the hydrostatic stress, and $Q(hkl)$ is the product of the supported differential stress and the elastic compliance relevant for the indicated (hkl) lattice plane. Under constant stress boundary conditions,

$$Q(hkl) = \frac{t_{\text{diff}}}{6G_{\text{Reuss}}(hkl)}, \tag{2}$$

where t_{diff} is the differential stress (difference between the maximum principal stress along the diamond axis and the minimum principal stress along the gasket direction) G_{Reuss}(hkl) is the lattice-dependent constant stress bound on the aggregate shear modulus. Under constant strain boundary conditions, Eq. (2) becomes

$$Q(hkl) = \frac{t_{\text{diff}}}{6G_{\text{Voigt}}}. \tag{3}$$

Note that the constant strain boundary aggregate shear modulus G_{Voigt} is not lattice-plane dependent. For an elastically isotropic material, $G_{\text{Reuss}}=G_{\text{Voigt}}$; for a material with low elastic anisotropy, the bounds on the shear moduli are similar so that the average of the (hkl)-dependent G_{Reuss} values is approximately equal to G_{Voigt}.

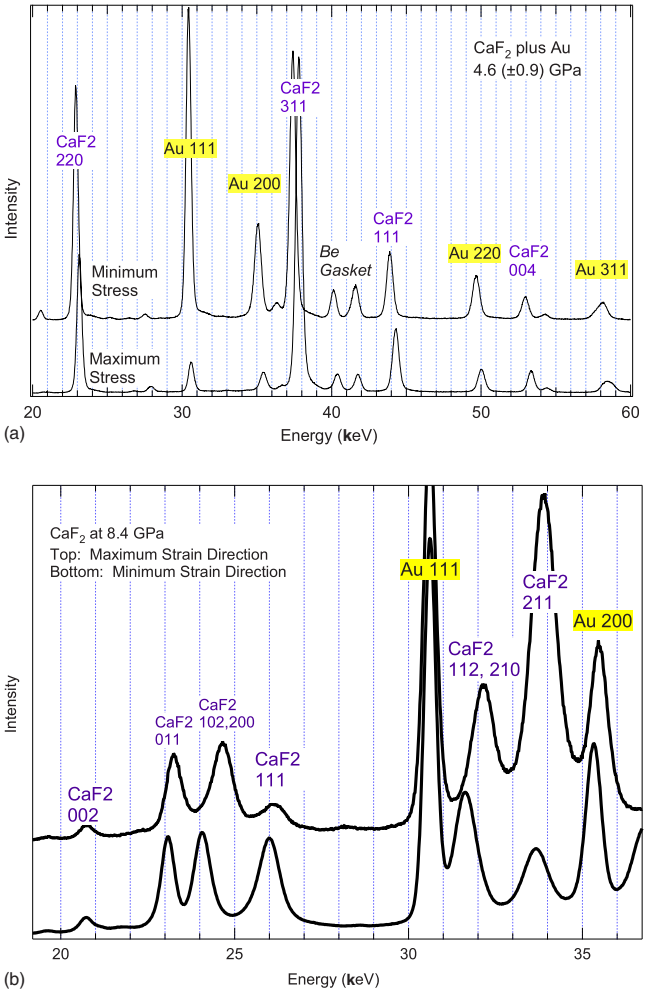

FIG. 1. (Color online) (a) Diffraction patterns in the minimum and maximum stress direction for low-pressure phase of CaF_2 (fluorite) and gold at 4.9 GPa. Diffraction peaks for both phases are labeled. Two peaks corresponding to diffraction from the Be gasket are shown. (b) Portion of diffraction patterns in the minimum and maximum stress directions for high-pressure orthorhombic phase of CaF_2 and gold at 8.4 GPa. Diffraction peaks for both phases are indexed.

IV. RESULTS

The first four pressure steps show x-ray diffraction patterns corresponding to gold and the cubic fluorite phase. Each diffraction pattern was indexed by assigning the appro-

TABLE I. Fluorite (low-pressure CaF_2) lattice parameters calculated from measured d spacings in diffraction patterns. Values are in Å. Precision of each number is $\sim 10^{-5}$. Pressures (in GPa) are determined from values for Au (see text).

Pressure	Ψ angle	(111)	(220)	(311)	(400)
0.57 (±0.08)	Diamond axis	5.459	5.448	5.456	
	90	5.444	5.45	5.456	
	180	5.439	5.435	5.444	
3.49 (±0.17)	180	5.408	5.401	5.401	
	90	5.354	5.351	5.354	
	70	5.363	5.36	5.362	
	110	5.363	5.362	5.362	
	130	5.38	5.377	5.378	
	200	5.396	5.391	5.391	
4.58 (±0.87)	90	5.326	5.32	5.326	5.333
	0	5.381	5.378	5.374	5.373
	30	5.36	5.361	5.36	
	50	5.34	5.34	5.344	
	70	5.331	5.328	5.331	
	110	5.33	5.331	5.331	
	−30	5.366	5.363	5.363	
	90	5.294	5.296	5.299	
7.09 (±2.05)	90	5.296	5.297	5.300	
	180	5.349	5.347	5.345	
	150	5.333	5.336		
	120	5.311	5.31	5.315	
	120	5.314	5.313	5.314	
	70	5.298	5.299	5.31	

priate Miller index corresponding to Au (111, 200, 220, and 311 peaks) and fluorite (111, 220, 311, and 400) peaks. The two highest pressure steps showed gold and high-pressure CaF_2, which was indexed following the orthorhombic structure determined by Morris *et al.*[7] and using the following diffraction peaks: (002), (011), (102)/(200) (overlapping peaks), (111), (112)/(210), and (211). The Gaussian fit subroutine in IGOR (www.wavetrics.com) was used to individually determine the center energy position of each diffraction peak. Typical precisions in the fit of the peak position were 0.4 eV, corresponding to one part in 10^{-5}. For each diffraction peak, the corresponding d spacings were calculated using Bragg's law. For the cubic fluorite phase, lattice parameters corresponding to each (hkl) were calculated (Table I). The (hkl)-dependent d spacings were tabled for the high-pressure phase (Table II).

For the cubic fluorite phase, each d spacing provides an independent measurement of the lattice constant. These lattice constants are plotted as a function of $1-3\cos^2\psi$ in Fig. 2 for the low-pressure cubic fluorite phase, and the data are analyzed as outlined in Sec. III. For a sample with a cylindrically symmetric stress tensor oriented along the diamond cell axis, the hydrostatic component of the stress in the sample is equal to $1/3(2\sigma_{\min}+\sigma_{\max})$, where $\sigma_{\min}$ and $\sigma_{\max}$ are the minimum and maximum principle stresses. Under this assumption, the d spacing at $1-3\cos^2\psi=0$ (the y intercept) is the hydrostatic component of the lattice response.

In Secs. V and IX, the hydrostatic information is evaluated and interpreted in terms of a P-V equation of state for CaF_2, the inferred lattice strength for both gold and CaF_2 is estimated, and the lattice-plane strain anisotropy is investigated. Finally, we explore the rheological behavior of the high-pressure assemblage as CaF_2 undergoes a pressure-induced phase transformation.

V. PRESSURE-VOLUME EQUATION OF STATE AND STRUCTURE OF CaF_2

Au is used as an independent pressure marker to infer the hydrostatic stress state within the sample chamber. As a starting point, this analysis assumes that the pressure experienced by Au is equal to that experienced by CaF_2. This assumption will be revisited in the last part of this section. At each pressure step, the hydrostatic value of each (hkl) diffraction line was determined by fitting the data in Table III to Eq. (1). Since Au is isometric, each lattice plane of Au provides an

TABLE II. Measured d spacings for the high-pressure phase of CaF_2. Values are in Å.

Pressure	Ψ angle	(002)	(011)	(102/200)	(111)	(112/210)	(211)
8.8 (±0.14)	90	3.403	3.041	2.873	2.719	2.205	2.093
	90	3.404	3.039	2.870	2.716	2.203	2.090
	90	3.404	3.037	2.866	2.709	2.200	2.088
	70	3.400	3.038	2.856	2.714	2.199	2.084
	110	3.400	3.039	2.852	2.712	2.198	2.080
	140	3.400	3.056	2.921	2.725	2.219	2.098
	210	3.415	3.071	2.937	2.734	2.230	2.104
	180	3.426	3.080	2.955	2.737	2.248	2.113
	180	3.424	3.082	2.956	2.735	2.248	2.113
	90	3.379	3.039	2.859	2.699	2.192	2.082
11.48 (±0.22)	180	3.408	3.079	2.945	2.721	2.241	2.098
	90	3.380		2.809	2.676	2.153	2.058

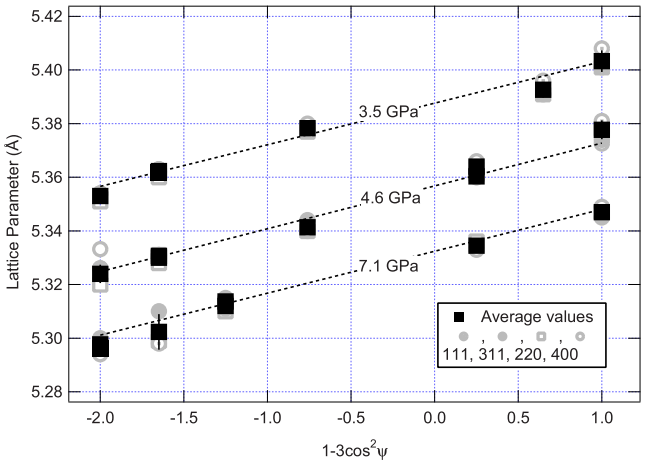

FIG. 2. (Color online) Lattice parameters corresponding to the observed (111), (311), (220), and (400) lattice planes of CaF_2 fluorite (gray symbols) plotted as a function of linearized diamond cell azimuthal angle $1-3\cos^2\psi$ at three different pressure steps (labeled). The average of (*hkl*)-dependent values at each azimuthal position and pressure is plotted as a black square. Standard deviations are shown as the vertical error bars; some are within the height of the symbol. Weighted linear least square fits through these average values are plotted as dashed lines. Pressures are from values calculated for Au.

independent estimate of the hydrostatic component of the lattice parameter. Cell volumes and one-sigma uncertainties were then calculated from the average value and standard deviations of the (*hkl*)-dependent lattice parameters. At each pressure step, a pressure and associated error was calculated from the average volume and standard deviation using a third-order Birch–Murghnahan equation of state, assuming $K_0=167$ GPa and $dK_0/dP=5.8$,[16,17] equation of state to generate the corresponding hydrostatic pressure and one-sigma uncertainties at each step. The resulting pressures determined by Au at each step were 0.57(±0.08)GPa, 3.49(±0.17)GPa, 4.58(±0.87)GPa, 7.09(±2.05)GPa, 8.8(±0.14)GPa, and 11.48(±0.22)GPa.

Throughout the first four pressure steps, CaF_2 is in the cubic fluorite structure, and the hydrostatic volumes are determined following the approach for Au. Results are plotted in Fig. 3. In the fluorite phase, the measured hydrostatic volumes as a function of pressure are in excellent agreement with the high-pressure $P(V)$ equation of state determined by Brillouin spectroscopy for CaF_2 (Ref. 18): $K_{0\,T}=82$ GPa and $dK/dP=4.83$. By the fifth pressure step (8.8 GPa) fluorite has undergone a phase transformation to the higher pressure orthorhombic phase as evidenced by changes in the diffraction pattern observed in all directions [Fig. 1(b)]. Therefore, this study constrains the phase transformation pressure to occur between pressures of 7.1 and 8.8 GPa, in agreement with previous estimates of the phase transformation which span the range of 7.75–10 GPa.[8,18,19]

We analyze the diffraction pattern based on the *Pnma* structure and atomic positions following the structural determination by Morris *et al.*[7] Indexed measured diffraction patterns from the minimum and maximum stress directions are shown in Fig. 1(b). At each pressure step and at each ψ angle, these lattice planes were used to provide best-fit lattice parameters for the orthorhombic structure using the regression analysis package provided by EXCEL. Then, the regressed values of the *a*, *b*, and *c* lattice parameters were plotted as a function of $1-3\cos^2\psi$ (Ref. 2) (Fig. 4). A weighted least-squares linear fit determined the hydrostatic value and *Q* value for each of the lattice parameters. The hydrostatic component of the volume was calculated from the hydrostatic components of the *a*, *b*, and *c* lattice parameters and is plotted in Fig. 3 as a function of pressure determined by Au. At 8.8 GPa, the hydrostatic volume of the high-pressure phase is 133.6±2.15 Å.[3] According to the

TABLE III. Gold lattice parameters calculated from measured *d* spacings in diffraction patterns at all pressure steps. Values are in Å. Precision of each number is $\sim 10^{-5}$.

Pressure	Ψ angle	(111)	(220)	(311)	(400)
0.57 (±0.08)	Diamond axis	4.078	4.079	4.077	4.078
	90	4.071	4.068		4.071
	180	4.072	4.071	4.072	4.073
3.49 (±0.17)	180	4.057	4.063	4.058	4.062
	90	4.036	4.026	4.034	4.035
	70	4.04	4.03	4.038	4.051
	110	4.039	4.031	4.036	4.037
	130	4.045	4.043	4.043	4.046
	200	4.055	4.06	4.056	4.088
4.58 (±0.87)	90	4.025	4.013	4.022	4.033
	0	4.048	4.056	4.05	4.063
	30	4.04	4.042	4.04	4.049
	50	4.033	4.03	4.032	4.049
	70	4.027	4.017	4.025	4.025
	110	4.026	4.021	4.023	4.028
	−30	4.042	4.049	4.044	4.064
	90	4.025	4.013	4.022	4.033
7.09 (±2.05)	90	4.016	3.999	4.012	4.019
	180	4.017	4.000	4.013	4.019
	150	4.032		4.033	4.057
	120	4.026		4.026	4.05
	120	4.015	4.003	4.019	4.025
	70	4.016	4.004	4.021	4.026
		4.017	4.004	4.015	4.021
8.8 (±0.14)	90	4.00633	3.995	4.001	3.999
	90	4.00646	3.996	4.002	3.999
	90	4.00685	3.998	4.002	3.999
	70	4.00437	3.990	4.003	3.996
	110	4.00281	3.998	4.009	3.994
	140	4.00841	4.015	4.005	4.005
	210	4.01403	4.020	4.014	4.017
	180	4.02255	4.027	4.027	4.027
	180	4.02268	4.028	4.028	4.027
	90	4.00698			
11.48 (±0.22)	180	3.987	3.978	3.98	3.979
	90	4.005	4.013	4.007	4.01

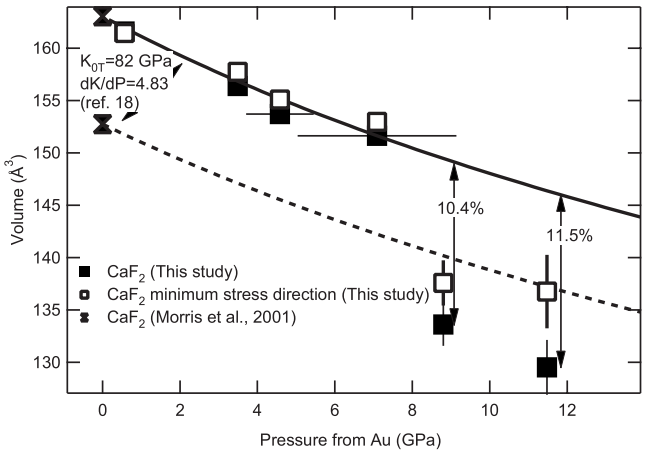

FIG. 3. Measured unit cell volumes as a function of pressure for CaF_2. The solid squares are volumes at the hydrostatic conditions. The open squares are volumes inferred from strains in the minimum stress direction. The symbols at zero pressure are from Morris *et al.* (Ref. 7). The solid curve shows calculated $P(V)$ compressibility from Ref. 18. The dotted curve shows the same compressibility using the zero pressure value Morris *et al.* (Ref. 7) as V_0. Pressure is determined by using the lattice parameters of Au. The measured $\Delta V=(V_2\text{-}V_1)/V_1$ for the transition between the high-pressure phase and low-pressure phase are shown at the two highest pressure steps.

fluorite equation of state, the corresponding volume in the low-pressure phase is 149.4 Å.[3] This generates a volume decrease equal to $(V_2\text{-}V_1)/V_1$=equal to $10.4\pm1.5\%$. This value is consistent with, but on the high side of, the 7%–10% range predicted by theoretical studies[4,5] and determined by many of the experimental studies, which have values from 6.3% to 11%.[8,19] At the next pressure step, the volume jump is $11.5\pm(2.0)\%$ at 11.5 GPa.

Although our two high-pressure data points are not sufficient to constrain an estimate for the bulk modulus of the high-pressure phase, our observation of increasing volume jump with pressure suggests that the high-pressure phase may be more compressible than the low-pressure phase. However, this observation is not well constrained within error bars and is at odds with static simulations combining first-principles pairwise simulations and quantum mechanical *ab initio* perturbed ion calculations[4,6] of the high-pressure structure. However, a decrease in bulk modulus after a phase transformation is observed in other systems, such as across the B1–B2 phase transformation of NaCl.[20–23]

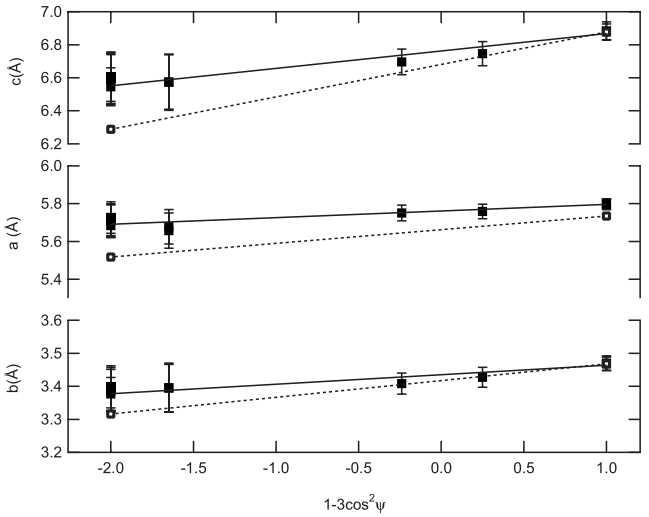

FIG. 4. The orthorhombic lattice parameters a, b, and c for CaF_2 at 8.8 GPa (solid squares) and 11.5 GPa (open squares) are plotted as a function of azimuthal angle Ψ. Weighted linear fits are shown as the solid lines (8.8 GPa) and dotted lines (11.5 GPa).

To examine the extent to which this volume jump is sensitive to differential stress, we examined the apparent lattice volume determined in the minimum stress direction, which corresponds to what would be observed if x-ray diffraction were done the diamond cell axis direction. These data, which imply a much larger cell volume than in the hydrostatic direction, are plotted in Fig. 3. The corresponding volume decreases for the lattice parameter determined in the minimum stress directions are equal to 7.9% and 6.6%. The difference between the hydrostatic volume decrease and the decrease inferred in the minimum stress direction is large because this experiment was designed to maximize nonhydrostatic stresses in the diamond cell. However, the presence of even small nonhydrostatic stress will generate an underestimate of the volume change in a phase transformation. Therefore, it is possible that previous experimental measurements provided underestimates of the volume collapse due to the presence of small amounts of nonhydrostaticity, which is possible even in methanol:ethanol mixtures.[24]

The radial-diffraction method also provides more detailed structural information about the high-pressure phase under varying stress and strain conditions. The orthorhombic *Pnma* structure of the high-pressure phase of CaF_2 can be considered as a distortion of an hexagonal close pack lattice. The ideal hcp lattice has a/b and c/b ratios of 1.6333 and 1.732, which lies down and far to the left of the origin of the plot in Fig. 5. The measured a/b and c/b axes ratios provide insight into the structure and provide a means to cross compare structures.[7] Figure 5 shows the a/b and c/b ratios plotted for our two highest pressure data sets, in the minimum, maximum, and hydrostatic stress directions. Several trends are apparent. First, the c/b ratio experiences significant shift downward as the sample is rotated from minimum to maximum stress direction. The a/b ratio shows a smaller shift upward. However, with increasing pressure, the a/b ratio decreases for all directions. In the maximum stress direction, the c/b ratio decreases with increasing pressure; however, in the minimum stress direction, it remains approximately constant. The lattice parameter ratios determined by Morris *et al.*[7] were determined by quenching from pressures of 8.6 GPa, close to our measurement at 8.8 GPa; their values are intermediate between the two hydrostatic values determined here and well within mutual uncertainties.

VI. ELASTICALLY SUPPORTED DIFFERENTIAL STRESS OF GOLD AND CaF_2

For the cubic phases, a lattice-averaged elastically supported differential stress is estimated by averaging values for each lattice plane via

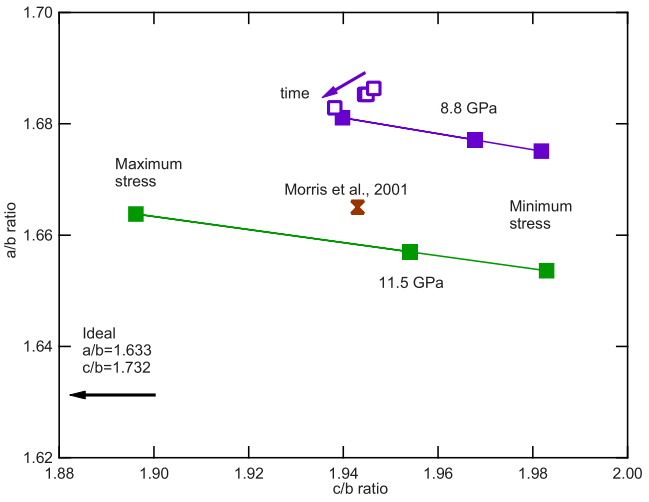

FIG. 5. (Color online) Measured a/b and c/b lattice parameter ratios for CaF_2 in the high-pressure phase at maximum, minimum, and hydrostatic stress conditions. Structural relaxation in the maximum stress direction at 8.8 GPa is shown as the open squares with an arrow indicating time progression. Also shown is the measurement of Morris *et al.* (Ref. 7). The lattice parameter ratios corresponding to an ideal hexagonal close pack lattice is indicated by the black arrow.

$$t_{\text{diff}} = 6G_{\text{VRH}}\langle Q(hkl)\rangle, \tag{4}$$

where G_{VRH} is the Voigt–Reuss–Hill average of the aggregate shear moduli. High-pressure shear moduli for Au were calculated using $G_{\text{VRH}}=27.6$ GPa with $dG/dP=1.05$.[25] For fluorite, values of $G_{\text{VRH}}=42.8$ GPa and $dG/dP=1.08$ (Ref. 18) were used. The results calculated for differential stress are shown as a function of pressure in Fig. 6. At the first pressure step, which was obtained with almost no compression in the diamond cell, neither Au nor CaF_2 show significant values for supported differential stress (-0.08 ± 0.11 for CaF_2 and 0.07 ± 0.02 for Au). At elevated pressures, the differential stress found for Au averages ~0.47 GPa across the pressure range, in general agreement with values measured by Duffy *et al.*,[9,10] but systematically higher than the average values published in those studies (solid gold line in Fig. 6). In the low-pressure phase, fluorite supports a uniform differential stress of 0.82 GPa. The observation that both Au and fluorite show constant differential stress values as the pressure is increased suggest that both of these materials are at their elastic limit, no work-hardening occurs, and we interpret these values as a yield strength for each material.

Figure 4 shows that the individual lattice constants of the high-pressure phase of CaF_2 are strongly dependent on Ψ, with the c axis showing far more variation than either a or b axes as the orientation progresses from minimum to maximum stress direction. The Q strain values determined for each lattice parameter are 6×10^{-3}, 8.4×10^{-3}, and 15.6×10^{-3} for the a, b, and c parameters, respectively. These are large values compared with the average value for the cubic fluorite phase, 2.9×10^{-3}. Independent of single-crystal symmetry, the supported differential stress is related to the product of the measured $\langle Q\rangle$ value and the appropriate lattice-dependent shear modulus, as shown in Eqs. (1)–(3). Therefore, the high measured Q values imply either that the high-pressure phase of CaF_2 has a high t_{diff} or low values of G compared to the low-pressure fluorite phase. Although a complete determination of differential stress for the high-pressure phase requires knowing the full complement of elastic moduli, we can use Eqs. (2) and (3) to calculate an approximate lattice-average differential stress for the high-pressure phase using an aggregate value for G. No experimental measurements yet exist for this value; however, a theoretical calculation of the shear moduli of the high-pressure phase of CaF_2 (Ref. 26) provides values of 43 GPa at 0 K and 10 GPa lowering to ~40 GPa at 300 K. Therefore, we use this aggregate value for the shear modulus of the orthorhombic CaF_2 phase and extrapolate in pressure using the dG/dP value of the low-pressure fluorite phase, 1.08. The lattice strength values inferred for the three lattice parameters, ignoring elastic anisotropy, are plotted on the top part of Fig. 6. For the a axis, the values range from 2 to 4 GPa at 8.4 to 11.1 GPa of pressure. For the c axis, the values range from 5 to 10 GPa over the same pressure range. These values are approximate; however, the enhanced ability of the high-pressure phase to support a differential stress is apparent, as is the lattice anisotropy of the high-pressure phase.

To our knowledge, this observation of phase-boundary strengthening is unique. In observations of supported differential stress across the SiO_2 phase boundary,[27] phase-change strengthening was not observed. One possible explanation is that strengthening arises from a decrease in grain size during nucleation of the new high-pressure phase. However, this must be tested with more experiments. The apparent increase in strength for the high-pressure phase relative to the low-pressure phase of CaF_2 is especially interesting when contrasted with the corresponding apparent decrease of bulk modulus in the high-pressure phase. This behavior runs counter to the idea that high bulk modulus may be a proxy for high material yield strength.[28]

The second important result is the strongly anisotropic lattice response in the supported differential stress, with the azimuthal strain response increasing from the a to b to c parameters. This directional dependence is either due to elastic anisotropy in the high-pressure phase (and also therefore implies significant elastic anisotropy) or a result of yield strength anisotropy of the lattice. Without independent measures of the elastic constants and elastic anisotropy of the high-pressure form of CaF_2, these two possibilities are not easily distinguished. Elastic anisotropy will be considered further in Sec. VII.

VII. LATTICE ANISOTROPY OF Au AND FLUORITE

Differences in the strain behavior of different sets of lattice planes provide additional information about the elastic anisotropy of the lattice. Although it has been shown that lattice anisotropy can originate because of directional plastic behavior,[29] here we assume that the lattice anisotropy has an elastic origin and attempt to use the lattice-plane-dependent strain to estimate this value. The measured lattice strain anisotropy can be related to the single-crystal elastic properties

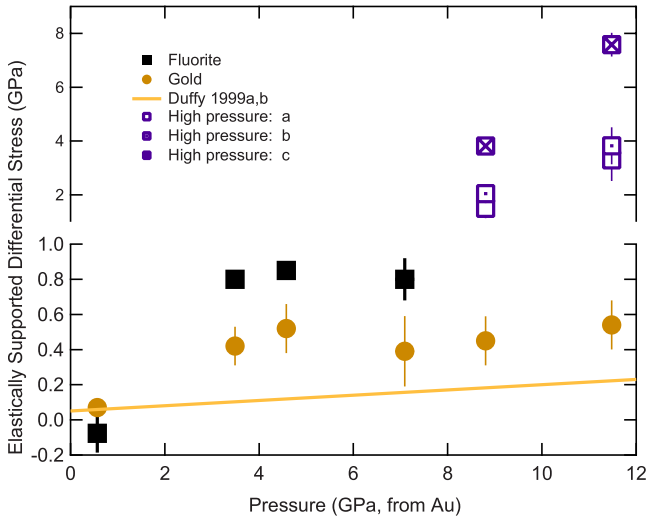

FIG. 6. (Color online) Differential stress as a function of pressure for CaF_2 and Au. The solid gold line is from a linear fit through the Au radial-diffraction data from Duffy *et al.* (Refs. 9 and 10). The high-pressure phase supports more differential stress. Note that the *y*-axis scale changes to encompass the much larger values of the differential stress supported by the high-pressure phase.

taking into consideration the crystal symmetry group. For a cubic material under constant stress conditions, there are three independent elastic constants. Under constant stress conditions, the lattice elastic anisotropy is at its maximum, and $G_{\mathrm{Reuss}}(\mathrm{hkl})$ from Eq. (2) is equal to

$$\frac{1}{2G_R} = S_{11} - S_{12} - 3S\Gamma(hkl),$$

where

$$S = S_{11} - S_{12} - \frac{1}{2}S_{44}, \tag{5}$$

and

$$\Gamma(hkl) = \frac{h^2k^2 + h^2l^2 + k^2l^2}{(h^2 + k^2 + l^2)^2},$$

where S_{ij}'s are the single-crystal elastic compliances. Therefore, for a cubic material, the slope of a plot of $Q(hkl)$ vs G provides a measurement of elastic anisotropy. Here, we define elastic anisotropy as the ratio

$$\frac{S_{11} - S_{12}}{2S_{44}} = \frac{2C_{44}}{C_{11} - C_{12}}, \tag{6}$$

where *Cij*'s are the single-crystal elastic moduli. An elastically isotropic material has an anisotropy of 1 using this scale.

The elastic anisotropies determined in this manner for Au and for CaF_2 are plotted in Fig. 7. The measured elastic anisotropy for fluorite decreases slightly from 0.78 to 0.68 over the pressure range of 3.5–7.5 GPa. The average value of 0.73 is in superb agreement with the value of 0.733 measured by Brillouin spectroscopy.[18] Therefore, we conclude that the constant stress conditions that were assumed to interpret these anisotropy measurements is relevant, at least for the low-pressure fluorite phase.

VIII. BEHAVIOR OF GOLD AND CONSIDERATION OF PRESSURE ENVIRONMENT IN THE DIAMOND ANVIL CELL SAMPLE CHAMBER

For Au, most of the measurements of elastic anisotropy have the opposite sense, with an average value of 1.84. This value is far below the anisotropy value determined for single-crystal Au by ultrasonic measurements, which is equal to 3.0; however, it is identical within error bars to previous radial-diffraction measurements of Au.[9,10] One possibility for this discrepancy between the radial-diffraction measurements of Au's lattice anisotropy and the ultrasound values may be that the Au powder does not have a constant stress aggregate response but rather has an intermediate response between constant stress and constant strain boundary conditions.

The data also indicate that the continuity environment undergoes changes during the experiment, especially as CaF_2 undergoes its phase transformation. An anomalously low value for the elastic anisotropy measured for Au is observed at the pressure step immediately preceding the phase transformation in CaF_2; however, only a small decrease is observed in the corresponding supported differential stress. If both the differential stress and measured anisotropy were approaching zero prior to the phase transformation, it would imply that the environment in the sample chamber is approaching hydrostaticity at that point, presumably because of shear softening in the CaF_2, which is the volumetrically dominant phase. Since Au is retaining close to the same differential stress, the drop in observed anisotropy suggests that this phase is experiencing a transient shift from constant stress (Reuss) boundary conditions to constant strain (Voigt) boundary conditions.

The above observations have several interesting implications. First of all, they imply that the boundary conditions in these composite samples are exquisitely sensitive to the samples—likely a combination of their geometry, their relative strengths, and their elastic properties.[30] This may pose problems for measurements of elastic properties of materials in the diamond anvil cell sample chamber. From a practical point of view for high-pressure experiments, this observation suggests that the assumption of pressure continuity in the diamond cell must be thrown out or at least seriously interrogated.[31] If Au has a tendency to lose its anisotropic signature depending on the sample environment, this will pose problems for studies which use measured lattice strain anisotropy as a marker for nonhydrostaticity within the sample chamber.[32,33]

When polycrystalline materials inside a sample chamber are considered as composite materials, it is tacitly recognized that the stress environment inside the sample chamber does not require that the hydrostatic stress supported by Au is identical to that supported by CaF_2. The complete solution to the composite problem of samples inside the diamond cell requires a nonequilibrium polycrystalline plasticity model—which would have to be extremely sophisticated to account for the behavior. In these experiments, the assumption that

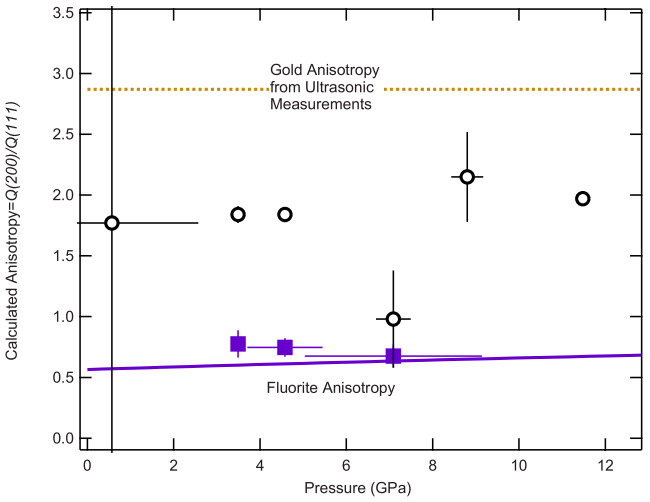

FIG. 7. (Color online) Elastic anisotropy measured for gold (yellow square symbols) and fluorite (purple square symbols). Room pressure ultrasonic values for gold are shown as a solid line. The measurements for gold underestimate the measured anisotropy, lower than the ultrasonic value, but in agreement with the radial-diffraction result of Duffy *et al.* (Refs. 9 and 10). The purple line shows the Brillouin scattering measurement for fluorite anisotropy by Speziale and Duffy (Ref. 18).

the pressure of Au and CaF_2 are equal is required to determine the equation of state of both materials; however, the estimates of differential stress and elastic anisotropy are not strongly influenced by this assumption.

IX. TIME-DEPENDENT RESPONSE

A further indication of the nonequilibrium environment in the diamond cell sample chamber, especially at or near a phase transformation, is seen in our data set, in which a series four measurements were obtained for the sample at 8.5 GPa in the maximum strain orientation over a time scale of ~12 h. Time-dependent lattice parameters for the Au (111) and (200) lines and for the *a*, *b*, and *c* lattice parameters of the high-pressure CaF_2 are shown in Figs. 8(a) and 8(b). Time is determined from the time of increasing the pressure on the diamond anvil cell—there is an offset of several minutes which was required to align the diamond cell for x-ray analysis.

Since these measurements were taken in the maximum stress direction, the evolution of the gold lattice parameter suggests that the gold is evolving toward the hydrostatic value, as expected for a sample undergoing viscous relaxation and therefore evolving toward hydrostaticity. This approach toward hydrostatic behavior is also indicated by the observation that the lattice parameters indicated by the (111) and (200) lines are approaching other in time, indicating a decrease in t_{diff} (assuming anisotropy and stress and/or stain continuity condition is constant with time). Following the discussion in Kavner and Duffy,[13] a transient creep viscosity can be estimated from this relaxation using the relation

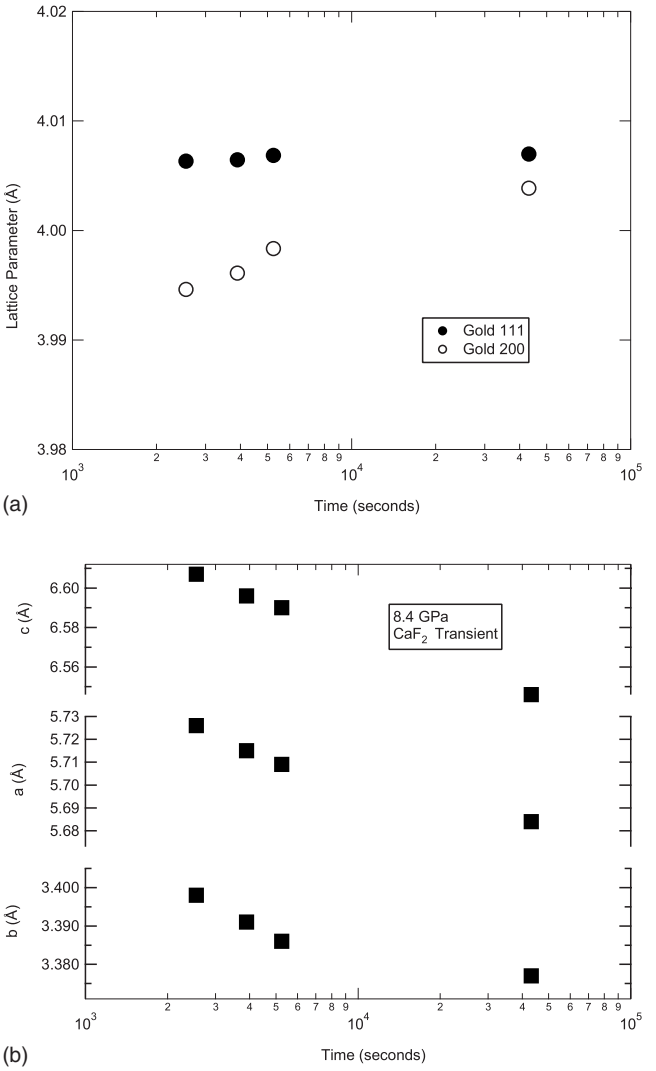

FIG. 8. High-pressure (a) gold and (b) CaF_2 lattice parameters in the maximum stress directions as a function of time for $P = 8.4$ GPa (average hydrostatic pressure of Au). All the *y* axes are scaled so that each scale represents a 1% range. For CaF_2, the lattice parameters are all decreasing with time, indicating a time-dependent shrinking of the lattice. The Au, on the other hand, shows the lattice parameters indicated by (111) and (200) are increasing, indicating a relaxation of the lattice toward the hydrostatic value. In addition, the (111) and (200) lattice strains are evolving toward each other, which provides a second indication of time-dependent relaxation of differential stress.

$$\eta = \frac{t_{\mathrm{diff}}}{\dot{\varepsilon}}, \tag{7}$$

where η is the dynamic viscosity, t_{diff} is the supported differential stress, and $\dot{\varepsilon}$ is the measured strain rate. The measured total strain of 0.03% over a ~12 h time scale and the measured differential stress of ~0.4 GPa indicate a dynamic viscosity of $\sim 7 \times 10^{16}$ Pa s. This is approximately an order of magnitude higher than the dynamic viscosity inferred for Pt under similar radial-diffraction conditions ($\sim 10^{15}$ Pa s).[13] These measurements are interesting; in that, they suggest that

very large viscosities may be accessible by radial-diffraction measurements.

In contrast, while the Au lattice is relaxing toward the hydrostatic value, the lattice parameters of orthorhombic CaF_2 are all decreasing as a function of time—and the observed strain rate (0.06%–0.07% strain over the same time period) is much larger than that for Au. Figure 8 also shows that the a/b and c/b ratios are evolving as a function of time. The a/b value is evolving toward the measured hydrostatic value; however, the c/b ratio is evolving away from the hydrostatic value over time. Interestingly, together, the ratios are evolving closer toward ideal hexagonal close packing with time, mirroring the behavior of the pressure evolution of CaF_2 in the maximum stress orientation. This volume relaxation cannot be interpreted simply as a viscous relaxation—since the sample volume is continuing to decrease, rather than increase toward is hydrostatic value. Our observed volume decrease over time—a 2.2% volume decrease over ~ 11 hours ($\sim 4 \times 10^4$ sec)—is in good general agreement with a study examining the kinetics of high-pressure phase transformation in CaF_2 (Ref. 19) using a strain gauge technique. However, their experiments were designed to examine the initial nucleation phase of the experiment at low overpressures, while our experiment sampled the final transient of the transformation at high overpressures. This strongly time-dependent behavior also may provide an explanation for previous overestimates of the high-pressure phase sample volume. If not enough time were provided for the equilibrium volume to be approached, then the lattice parameters for the orthorhombic structure would be systematically overestimated.

X. CONCLUSIONS

Radial-diffraction measurements continue to indicate that the stress environment in a diamond anvil cell is far from simply understood. The stress state experienced by the two samples mixed together—an unknown and a standard material—is in general different from each other, and the conditions for each may also be evolving throughout the course of an experiment, especially at a phase transformation. Even though these radial-diffraction measurements are designed to maximize differential stress, the effects of differential stress are likely to play a role even at conditions closer to hydrostaticity. This is important to take into consideration when making measurements in the diamond anvil cell at high pressures and temperatures because it may complicate measurement of phase stability and equation of state.

On the other hand, radial-diffraction techniques provide a window into important behavior of composite materials subjected to extreme hydrostatic and differential stresses in the diamond anvil cell. These results on CaF_2 also provide insight into mechanical behavior of a composite system during a phase transformation of one of the mechanical components. Stress behavior and strain behavior can be monitored for each phase separately in order to evaluate physical continuity of either stress or strain in the diamond cell. In addition, these results point to the possibility of examining viscous creep—strain transients—of materials subjected to high pressure in the diamond anvil cell.

ACKNOWLEDGMENTS

This research was supported by National Science Foundation under Grant No. EAR 0510914. The use of the National Synchrotron Light Source, Brookhaven National Laboratory was supported by the Office of Science, Office of Basic Energy Sciences, U.S. Department of Energy under Contract No. DE-AC02-98CH10886, and by COMPRES, the Consortium for Materials Properties Research in Earth Sciences under NSF Cooperative Agreement No. EAR 06-49658.

*akavner@ucla.edu

[1] F. Birch, J. Geophys. Res. **83**, 1257 (1978).
[2] N. Sata, G. Y. Shen, M. L. Rivers, and S. R. Sutton, Phys. Rev. B **65**, 104114 (2002).
[3] R. J. Angel, J. Phys.: Condens. Matter **5**, L141 (1993).
[4] A. M. Pendas, J. M. Recio, M. Florez, V. Luana, and M. Bermejo, Phys. Rev. B **49**, 5858 (1994).
[5] X. Wu, S. Qin, and Z. Y. Wu, Phys. Rev. B **73**, 134103 (2006).
[6] V. Kanchana, G. Valtheeswaran, and M. Rajagopalan, Physica B **328**, 283 (2003).
[7] E. Morris, T. Groy, and K. Leinenweber, J. Phys. Chem. Solids **62**, 1117 (2001).
[8] L. Gerward, J. S. Olsen, S. Steenstrup, M. Malinowski, S. Asbrink, and A. Waskowska, J. Appl. Crystallogr. **25**, 578 (1992).
[9] T. S. Duffy, G. Y. Shen, D. L. Heinz, J. F. Shu, Y. Z. Ma, H. K. Mao, R. J. Hemley, and A. K. Singh, Phys. Rev. B **60**, 15063 (1999).
[10] T. S. Duffy, G. Y. Shen, J. F. Shu, H. K. Mao, R. J. Hemley, and A. K. Singh, J. Appl. Phys. **86**, 6729 (1999).
[11] A. Kavner and T. S. Duffy, Geophys. Res. Lett. **28**, 2691 (2001).
[12] A. Kavner, Earth Planet. Sci. Lett. **214**, 645 (2003).
[13] A. Kavner and T. S. Duffy, Phys. Rev. B **68**, 144101 (2003).
[14] A. K. Singh, C. Balasingh, H. K. Mao, R. J. Hemley, and J. F. Shu, J. Appl. Phys. **83**, 7567 (1998).
[15] A. K. Singh, J. Appl. Phys. **73**, 4278 (1993).
[16] D. L. Heinz and R. Jeanloz, J. Appl. Phys. **55**, 885 (1984).
[17] O. L. Anderson, D. G. Isaak, and S. Yamamoto, J. Appl. Phys. **65**, 1534 (1989).
[18] S. Speziale and T. S. Duffy, Phys. Chem. Miner. **29**, 465 (2002).
[19] F. S. Yel'kin, O. B. Tsiok, V. V. Brazhkin, and L. G. Khvostantsev, Phys. Rev. B **73**, 094113 (2006).
[20] D. L. Heinz and R. Jeanloz, Phys. Rev. B **30**, 6045 (1984).
[21] A. M. Hofmeister, Phys. Rev. B **56**, 5835 (1997).
[22] D. Walker, L. M. D. Cranswick, P. K. Verma, S. M. Clark, and S. Buhre, Am. Mineral. **87**, 805 (2002).
[23] S. Froyen and M. L. Cohen, Phys. Rev. B **29**, 3770 (1984).
[24] J. W. Otto, J. K. Vassiliou, and G. Frommeyer, Phys. Rev. B **57**, 3253 (1998).
[25] S. N. Biswas, P. Vantklooster, and N. J. Trappeniers, Physica B & C **103**, 235 (1981).

[26] Z. Y. Zeng, X. R. Chen, J. Zhu, and C. E. Hu, Chin. Phys. Lett. **25**, 230 (2008).
[27] S. R. Shieh, T. S. Duffy, and B. S. Li, Phys. Rev. Lett.. **89**, 255507 (2002).
[28] M. L. Cohen, Science **261**, 307 (1993).
[29] D. J. Weidner and L. Li, J. Phys.: Condens. Matter **18**, S1061 (2006).
[30] N. Conil and A. Kavner, J. Appl. Phys.. **100**, 043517 (2006).
[31] N. Conil and A. Kavner, J. Phys.: Condens. Matter **18**, S1039 (2006).
[32] S. H. Shim, T. S. Duffy, and G. Y. Shen, J. Geophys. Res. **105**, 25955 (2000).
[33] S. H. Shim, T. S. Duffy, and G. Y. Shen, Phys. Earth Planet. Inter. **120**, 327 (2000).